PERGAMON

International Journal of Solids and Structures 38 (2001) 1605–1623

INTERNATIONAL JOURNAL OF SOLIDS and STRUCTURES

www.elsevier.com/locate/ijsolstr

# Spectral element technique for efficient parameter identification of layered media. I. Forward calculation

R. Al-Khoury, A. Scarpas *, C. Kasbergen, J. Blaauwendraad

*Section of Structural Mechanics, Faculty of Civil Engineering and Geosciences, Delft University of Technology, Stevinweg 1, 2628 CN Delft, Netherlands*

Received 28 December 1999; in revised form 7 April 2000

**Abstract**

This contribution deals with the use of spectral analysis as a means of analysing the dynamic behaviour of the axially symmetric multi-layered systems as a result of a transient force. The objective of this research work is to develop an accurate and computationally efficient forward tool suitable for solving inverse problems. The spectral element technique is utilized. Details of the mathematical derivation, implementation and verification of newly developed axisymmetric and half-space spectral elements are presented. It is shown that the suitability of the spectral element method to such a problem encompasses in its ability to model a whole layer without the need for subdivisions. As a consequence, the size of the modelled structure becomes as large as the number of the layers involved. This reduces the computational requirements substantially and hence enables efficient utilization of the method in iterative algorithms for solving inverse problems. 

*Keywords:* Spectral element; Finite element; Layered media; Wave propagation

## 1. Introduction

Non-destructive testing for parameter identification and structural evaluation is a widely used technique in many fields. Parameter identification problems involve *forward* as well as *inverse* techniques. Solving the forward problem requires structural and material models to predict the values of some response quantities (e.g. displacements) from the given values of the model parameters. Solving the inverse problem requires techniques to infer the values of the model parameters from measured values of the response quantities. In this paper, the forward model will be addressed. In a subsequent paper, the use of the forward model for parameter identification will be presented.

The objective of this research work is to develop an accurate and computationally efficient forward tool for analysing the dynamic behaviour of layered media. This tool will be utilized, in a later work, in an iterative algorithm for solving inverse problems. As an application, the case of pavement response under the action of a falling weight deflectometer (FWD) load pulse is examined.

* Corresponding author. Fax: +31-15-278-5767.
*E-mail addresses:* r.alkhoury@ct.tudelft.nl (R. Al-Khoury), a.scarpas@ct.tudelft.nl (A. Scarpas).

0020-7683/01/$ - see front matter 
PII: S0020-7683(00)00112-8

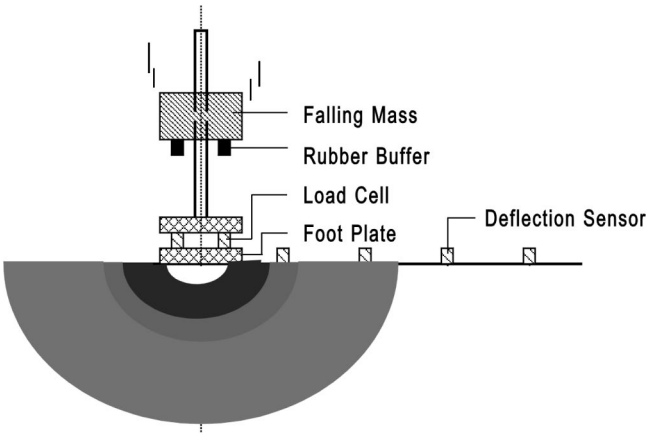


Fig. 1. Scheme of FWD instrument.

For roads and airfields the FWD (Fig. 1), is a commonly used non-destructive dynamic test for parameter identification of pavement layers. The FWD instrument consists of a large mass that is dropped from a certain height onto a set of rubber buffers mounted to a circular footplate (Van Gurp, 1995). The resulting impact approximates load effects of a truck wheel. Deflection sensors are used to record the vertical displacements at the surface at various radial distances from the loading centre. Maintenance strategies, in many countries all over the world, are based on the results of this test.

Commonly, either analytical or numerical methods are used for solving dynamic problems. Analytical methods usually imply exact solutions of wave propagation. They can be efficient for both forward and backward analyses. However, due to their nature, analytical solutions typically apply only to specific geometry and boundary conditions. In practice, various layer combinations and boundary conditions are encountered. Also, different instruments of different load characteristics are used in testing. All these render the analytical methods inept for utilization in practical applications.

Numerical methods and, in particular, the finite element method, is a general tool that can be used for the analysis of complex geometries and boundary conditions. However, and in spite of the recent advances in processor technology, powerful computing facilities are necessary even for problems of moderate size. This renders the finite element method difficult for utilization in inverse problems.

Over the years, many techniques have been developed for the analysis of wave motions in layered media. They involve combination of analytical and numerical solutions. Important work has been done by Thomson (1950) and Haskell (1953), who developed the layer transfer matrix method. For a given layer bounded between two interfaces, $j$ and $j+1$, this method relates the amplitudes of force vector $\{\hat{P}\}$ and displacement vector $\{\hat{U}\}$ at interface $j$ to those at interface $j+1$ by

$$\begin{Bmatrix} \hat{U}_{j+1} \\ \hat{P}_{j+1} \end{Bmatrix} = \begin{bmatrix} H_{11} & H_{12} \\ H_{21} & H_{22} \end{bmatrix} \begin{Bmatrix} \hat{U}_j \\ \hat{P}_j \end{Bmatrix}, \tag{1}$$

where $H_{ij}$ are submatrices of the transfer matrix (Haskell, 1953). Kausel and Roesset (1981) have further developed this method by introducing layer stiffness matrices analogous to those used in the finite element method by rearranging Eq. (1) to appear as

$$\begin{Bmatrix} \hat{P}_j \\ \hat{P}_{j+1} \end{Bmatrix} = \begin{bmatrix} -H_{12}^{-1}H_{11} & H_{12}^{-1} \\ H_{22}H_{12}^{-1}H_{11} - H_{21} & -H_{22}H_{12}^{-1} \end{bmatrix} \begin{Bmatrix} \hat{U}_j \\ \hat{U}_{j+1} \end{Bmatrix}. \tag{2}$$

Although this method adds no accuracy to the transfer matrix method, it is more efficient for numerical implementation due to the symmetry of the stiffness matrix (unlike that of the transfer matrix method). Kausel and Roesset provided continuous as well as semi-discrete solutions to the resulting system of dynamic equations. The continuous solutions describe wave motions in a layer in an exact form by solving a set of transcendental equations. However, these solutions exhibit, in some applications, instabilities due to the numerical complications involved in implementing infinite integration in computer codes. For example, in case of sharp variations in the stiffness of a layered system, a numerical oscillatory behaviour may occur during the contour integration of the displacement functions between zero and infinity in the spatial domain (Foinquinos et al., 1995). This occurs due to the singularities and/or the sharp peaks (depending on damping) that are encountered in the process.

A semi-discrete solution to such problems was first introduced by Lysmer (1970), who developed the lumped mass method for the analysis of Rayleigh waves in multi-layered elastic media. Later, this method was generalized by Kausel and Roesset (1981). Here, the wave motion is described exactly in the horizontal direction and approximately, by linear interpolation between the layer interfaces, in the vertical direction. The basic principle of the method is to divide the layer into sublayers with thickness smaller than the wavelengths of interest. This enables the substitution of the transcendental equations of the continuous technique with simple eigenvalue problems, which can be solved by standard techniques. This results to a more efficient numerical implementation. The layer stiffness matrix in this case is expressed as

$$\mathbf{K} = \mathbf{A}k^2 + \mathbf{B}k + \mathbf{G} - \omega^2\mathbf{M}, \tag{3}$$

where $k$ is the wavenumber, $\omega$ is the frequency of excitation, $\mathbf{A}$, $\mathbf{B}$, $\mathbf{G}$ are matrices of the material elastic properties and $\mathbf{M}$ is the lumped mass matrix. (Explicit expressions for the $\mathbf{A}$, $\mathbf{B}$, $\mathbf{G}$ and $\mathbf{M}$ matrices are given by Kausel and Roesset (1981)). Because the mass of the layer is lumped on the element's upper and lower interfaces, many elements are necessary for accurate description of the distribution of the mass.

Both the continuous and the semi-discrete techniques are suitable for the analysis of the far field problems. Tassoulas and Kausel (1983) have further extended these techniques to account for wave motions in finite regions with inhomogeneous boundary conditions caused by spatially finite loading. This method entails introducing specially developed elements under the loaded region and connecting them horizontally to the normal layer elements.

Because of the computational robustness of the semi-discrete formulation, compared with that of the continuous, it has been utilized in many engineering applications. However, the requirements for the subdivision of the layer elements and the introduction of additional elements for the simulation of the inhomogeneous regions result to a large system of equations that are to be solved. As a consequence, large amounts of computer time are needed, rendering these formulations "computationally expensive" for utilization in iterative schemes for solving inverse problems.

The spectral element method developed by Doyle (1997) combines elegantly the exact solution of wave motions with the finite element organization of the system matrices. In this, the system is solved by double summation over the involved frequencies and the wavenumbers (Rizzi and Doyle, 1992), alleviating thus the inconvenience of the numerical implementation of infinite integration. The mass distribution is modelled exactly and hence only one element is sufficient to describe a whole layer without the need for subdivisions. This makes the resulting system of dynamic equations very small and hence computationally efficient. Also, the method is suitable for both near field as well as far field problems, which makes it appropriate for FWD analysis.

In this article, the mathematical derivation, implementation and verification of a newly developed axisymmetric layer spectral element and a half-space spectral element are presented. The elements are utilized for the analysis of the dynamic behaviour of pavement structures under the impact of the FWD load pulse.

## 2. Wave motion in axi-symmetric systems

To describe wave motions in a solid medium, a homogeneous isotropic half-space $z \geqslant 0$ in the cylindrical co-ordinate system shown in Fig. 2 is considered. The system is assumed to be subjected at $z=0$ to a symmetrical normal load $P(r,t) = S(r)F(t)$ in which $S(r)$ represents its spatial distribution and $F(t)$ represents its time variation. Apparently, the wave motion generated by such load is axially symmetric.

### 2.1. Governing equations

The equations of motion of an isotropic linear elastic material can be expressed in terms of the displacements by use of Navier's equations

$$(\lambda+\mu)\nabla\nabla\cdot\mathbf{u}+\mu\nabla^2\mathbf{u}=\rho\ddot{\mathbf{u}}. \tag{4}$$

The vector $\mathbf{u}$ corresponds to the displacements of the material, $\rho$ is the mass density of the material and $\nabla$ indicates a vector differential operator; $\nabla\cdot\mathbf{u}$ is the divergence of $\mathbf{u}$ and $\nabla^2\mathbf{u}$ is the vector *Laplacian* of $\mathbf{u}$. $\lambda$ and $\mu$ are the Lamé constants expressed as

$$\lambda=\frac{vE}{(1+v)(1-2v)}, \qquad \mu=\frac{E}{2(1+v)},$$

where $E$ is Young's modulus and $v$ is Poisson's ratio.

In the Helmholtz decomposition, the displacement field of a material is expressed as the sum of the gradient of a scalar potential $\varphi$ and the curl of a vector potential $\boldsymbol{\psi}$ as

$$\mathbf{u}=\nabla\varphi+\nabla\times\boldsymbol{\psi}. \tag{5}$$

In an axi-symmetric motion, the vector potential $\boldsymbol{\psi}$ has a component $\psi_\theta$ only. This property reduces the solution of the problem to solving only for scalar potentials. For convenience of notation, $\psi$ will be written instead of $\psi_\theta$. Also, because of axi-symmetry, the displacement component in the $\theta$ direction is equal to zero. Denoting the displacement components in the $r$ and $z$ directions by $u$, and $w$, respectively, the relations between the displacement components and the potentials (Achenbach, 1973) are

$$u=\frac{\partial\varphi}{\partial r}-\frac{\partial\psi}{\partial z}, \tag{6a}$$

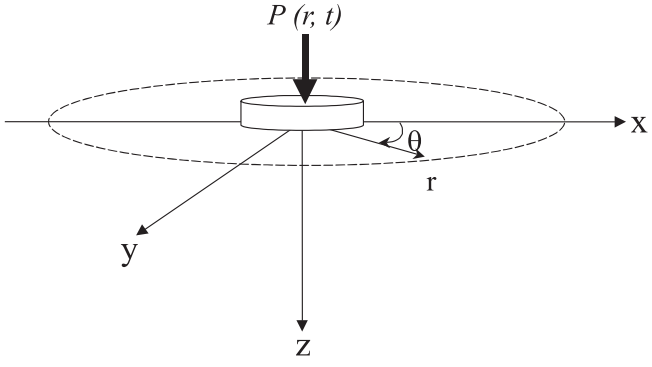


Fig. 2. Half space in cylindrical coordinate.

$$w = \frac{\partial \varphi}{\partial z} + \frac{1}{r}\frac{\partial (r\psi)}{\partial r}. \tag{6b}$$

The relevant stress–displacement relations are

$$\sigma_{zz} = (\lambda + 2\mu)\frac{\partial w}{\partial z} + \frac{\lambda}{r}\frac{\partial (ru)}{\partial r}, \tag{7a}$$

$$\tau_{zr} = \mu\left(\frac{\partial u}{\partial z} + \frac{\partial w}{\partial r}\right). \tag{7b}$$

By introducing Eq. (6) into Eq. (4), the above potentials satisfy the following axi-symmetric wave equations:

$$\frac{\partial^2 \varphi}{\partial r^2} + \frac{1}{r}\frac{\partial \varphi}{\partial r} + \frac{\partial^2 \varphi}{\partial z^2} = \frac{1}{c_p^2}\frac{\partial^2 \varphi}{\partial t^2}, \tag{8}$$

$$\frac{\partial^2 \psi}{\partial r^2} + \frac{1}{r}\frac{\partial \psi}{\partial r} + \frac{\partial^2 \psi}{\partial z^2} - \frac{\psi}{r^2} = \frac{1}{c_s^2}\frac{\partial^2 \psi}{\partial t^2}, \tag{9}$$

where the constants $c_p$ and $c_s$ are defined as

$$c_p = \left(\frac{\lambda + 2\mu}{\rho}\right)^{1/2}, \qquad c_s = \left(\frac{\mu}{\rho}\right)^{1/2}.$$

Eqs. (8) and (9) represent two basic types of waves; Compression (P) and Shear (S) waves respectively. Because of the isotropy, these waves are uncoupled from one another with each one being characterized by its specific velocity $c_p$ or $c_s$.

### 2.2. Constructing the potentials

In order to make no assumptions about the way the two waves propagate in the $r$ and $z$ directions, the potentials $\varphi$ and $\psi$ will be derived from the basic equations of motions (8) and (9). First, the solutions will be constructed for the scalar potential $\varphi$. An elegant way to solve the second degree partial differential equation Eq. (8) is by the use of Fourier transforms, which transform it from the time domain to the frequency domain as

$$-\omega^2 \hat{\varphi}(r,z) = c_p^2\left(\frac{\partial^2 \hat{\varphi}}{\partial r^2} + \frac{1}{r}\frac{\partial \hat{\varphi}}{\partial r} + \frac{\partial^2 \hat{\varphi}}{\partial z^2}\right). \tag{10}$$

The "hat" indicates that the expression is in the frequency domain. Solution of Eq. (10) can be obtained by the method of *separation of variables* (Kreyszig, 1999). Since $\hat{\varphi}$ is a function of the two orthogonal axes $r$ and $z$, the solution may consist of two independent functions of $r$ and $z$

$$\hat{\varphi}(r,z) = \hat{R}(r)\cdot\hat{Z}(z) \tag{11}$$

in which $\hat{R}(r)$ is a function of $r$ only and $\hat{Z}(z)$ is a function of $z$ only. On substituting Eq. (11) into Eq. (10), dividing through by $c_p^2\hat{R}(r)\hat{Z}(z)$ and equating both sides of the equation with some arbitrary constant, say $-k^2$, two independent ordinary differential equations for $\hat{R}(r)$ and $\hat{Z}(z)$ are obtained:

$$\frac{d^2\hat{R}(r)}{dr^2} + \frac{1}{r}\frac{d\hat{R}(r)}{dr} + k^2\hat{R}(r) = 0, \tag{12}$$

$$\frac{\mathrm{d}^2\hat{Z}(z)}{\mathrm{d}z^2}+\left(\frac{\omega^2}{c_\mathrm{p}^2}-k^2\right)\hat{Z}(z)=0. \tag{13}$$

If we set $s=kr$, then by use of the chain rule, Eq. (12) reduces to Bessel's equation

$$\frac{\mathrm{d}^2\hat{R}(s)}{\mathrm{d}s^2}+\frac{1}{s}\frac{\mathrm{d}\hat{R}(s)}{\mathrm{d}s}+\hat{R}(s)=0. \tag{14}$$

Solutions of Eq. (14) are the Bessel functions $J_0$ and $Y_0$ of the first and second kind. However, $Y_0$ becomes infinite at $r=0$, and since the oscillation is finite at the origin, the $Y_0$ solution is dropped and the solution of $\hat{R}(r)$ is left with

$$\hat{R}(r)=A_1J_0(s)=A_1J_0(kr), \tag{15}$$

where $A_1$ is a constant to be determined from the boundary conditions and $k$ represents the wavenumber in the radial direction. To discretize the problem, introduction of some boundary conditions in the radial direction is necessary. At the radial boundary $r=R$ (far away from the source) the amplitude of the oscillation is considered to vanish. Hence, the non-trivial solution of Eq. (15) becomes

$$\hat{R}(R)=J_0(kR)=0. \tag{16}$$

This condition can be satisfied at the infinitely many positive roots $\alpha_m$ of the $J_0$ function (Abramowitz and Stegun, 1972). Eq. (16) now implies $kR=\alpha_m$; thus $k=k_m=\alpha_m/R$. Hence, the $m$ functions,

$$\hat{R}_m(r)=A_{1m}J_0(k_mr)=A_{1m}J_0\left(\frac{\alpha_m}{R}r\right), \tag{17}$$

are solutions of the wave motion in the $r$ direction (Eq. (12)) that vanishes at $r=R$. Each function corresponds to the $m$th normal mode of vibration. It can be noticed here that the spatial boundary conditions at $r=R$ inevitably leads to a discrete set of wavenumbers of the normal mode vibrations.

In the case of $\hat{Z}$, the corresponding solution of Eq. (13) is

$$\hat{Z}_{mn}(z)=A_{2m}\mathrm{e}^{-\mathrm{i}k_{pzmn}z}, \tag{18}$$

where $A_{2m}$ is a constant, determined from the boundary conditions, i is the complex number $\sqrt{-1}$ and $k_{pzmn}$ represents the wavenumber in the vertical direction $z$ and is expressed as

$$k_{pzmn}=\left(\frac{\omega_n^2}{c_\mathrm{p}^2}-k_m^2\right)^{1/2}, \tag{19}$$

where $c_\mathrm{p}$ is the compression wave velocity and $\omega_n$ is the angular frequency. Thus, the solution of Eq. (11) for any given angular frequency $\omega_n$ is given by

$$\hat{\varphi}_{mn}(r,z)=A_{mn}\mathrm{e}^{-\mathrm{i}k_{pzmn}z}J_0(k_mr). \tag{20}$$

In the same way, the solution of the potential of the S wave $\hat{\psi}$ is

$$\hat{\psi}_{mn}(r,z)=B_{mn}\mathrm{e}^{-\mathrm{i}k_{szmn}z}J_1(k_mr), \tag{21}$$

where $B_m$ is a constant, determined from the boundary conditions, $J_1$ is the Bessel function of the first kind of order one and $k_{szmn}$ represents the vertical shear wavenumber and expressed as

$$k_{szmn} = \left( \frac{\omega_n^2}{c_s^2} - k_m^2 \right)^{1/2}, \tag{22}$$

where $c_s$ is the shear-wave velocity. These functions, $\hat{\varphi}_{mn}$ and $\hat{\psi}_{mn}$, are the eigenfunctions, or the characteristic functions, of the vibrating system and the values $k_m = \alpha_m/R$ are their eigenvalues. The vibration corresponding to $m$ is called the $m$th normal mode.

Eqs. (20) and (21) represent waves decaying exponentially in the $z$ direction and propagating horizontally in a Bessel's function mode. It is interesting to notice that travelling of the waves in the $z$ direction is analogous to that of the in plane structures (Rizzi and Doyle, 1992). However, in the horizontal direction, the harmonic (sinusoidal) waves of the plane condition become decaying waves of Bessel's function form in the axi-symmetric case.

## 3. Spectral double summation analysis of wave motion

The principle of superposition constitutes the core of the spectral analysis method. Since Eqs. (8) and (9) are linear and homogeneous, it follows from the superposition principle that the sum of *infinitely* many solutions $\hat{\varphi}_{mn}$ and $\hat{\psi}_{mn}$ (Eqs. (20) and (21)) are solutions of Eqs. (8) and (9), respectively. However, by use of the discretization technique of Section 2, double *summation over discrete* angular frequencies $\omega_n$ with $n = 1, \ldots, N$ and wavenumbers $k_m$ with $m = 1, \ldots, M$, is adequate to produce the overall vibration shape of the system that vanishes at $r = R$. The general solutions of wave equations in an axi-symmetric system are thus obtained by the superposition of all particular solutions to give

$$\varphi(r,z,t) = \sum_n \sum_m A_{mn} \mathrm{e}^{-\mathrm{i}k_{pzmn}z} J_0(k_m r) \mathrm{e}^{-\mathrm{i}\omega_n t}, \tag{23}$$

$$\psi(r,z,t) = \sum_n \sum_m B_{mn} \mathrm{e}^{-\mathrm{i}k_{szmn}z} J_1(k_m r) \mathrm{e}^{-\mathrm{i}\omega_n t}. \tag{24}$$

The limiting values of $N$ and $M$ can be determined from the amplitude spectrum of the time and spatial distribution of the loading pulse. As it will be shown later, the summation over $N$ frequencies can be carried out by use of the fast Fourier transforms (FFT) and the summation over $M$ wavenumbers can be done by use of the Fourier–Bessel series.

The double summation approach over Fourier series constitutes an essential computational advantage of this method over those, which rely on the numerical evaluation of integrals between zero and infinity. This type of integration involves singularities if the system has no damping or very sharp peaks for small damping, and it requires considerable computational time and capacity.

On substituting Eqs. (23) and (24) into Eqs. (6) and then Eqs. (7), by application of the boundary conditions, the displacements in an axi-symmetric medium can be expressed as

$$\left\{ \begin{matrix} w(r,z,t) \\ u(r,z,t) \end{matrix} \right\} = \sum_n \sum_m \hat{P}_{mn} \hat{G}(k_m, z) \left\{ \begin{matrix} J_0(k_m r) \\ J_1(k_m r) \end{matrix} \right\} \mathrm{e}^{\mathrm{i}\omega_n t} \tag{25}$$

in which $\hat{P}_{mn}$ is the amplitude spectrum depends on the spatial and the time variation of the load pulse, and $\hat{G}(k_m, z)$ represents the transfer function of the system. Eq. (25) reveals that summation over $M$ wavenumbers constructs the spatial dependency of the wave (oscillation shape) and summation over $N$ frequencies reconstructs the time dependency for that wave.

In the subsequent sections, the derivation of $\hat{G}(k_m, z)$ for layered axi-symmetric systems and the determination of $\hat{P}_{mn}$ for a circular-transient load pulse is presented.

## 4. Spectral axi-symmetric element formulation

The spectral element method (Doyle, 1997) is utilized for the formulation of axi-symmetric elements. Two spectral elements were developed: a 2-noded layer element and a 1-noded half-space element.

### *4.1. 2-Noded layer element*

The element can be pictorially presented to be consisting of two parallel circular surfaces within which the wave is constrained to move, Fig. 3. The element is physically defined by two nodes with each having one radial and one vertical degree of freedom. In the horizontal direction it extends to the distance $R$, where the wave motion vanishes, (Eq. (16)).

The response at any point in the element is determined by the superposition of incident waves and the reflected waves. An externally applied force generates the incident waves, which propagate, until they encounter the vertical boundary where reflected waves develop. The propagating waves in the element consist of a P-wave that travels with a speed $c_p$ and an S-wave that travels with a speed $c_s$. To include both the incident and reflected waves, the potentials at Eqs. (20) and (21) are adapted to include waves propagating in the negative $z$ direction as

$$\hat{\varphi}_{mn}(r,z,k_m,\omega_n) = \left(A_{mn}e^{-ik_{pzmn}z} + C_{mn}e^{-ik_{pzmn}(h-z)}\right)J_0(k_m r), \tag{26}$$

$$\hat{\psi}_{mn}(r,z,k_m,\omega_n) = \left(B_{mn}e^{-ik_{szmn}z} + D_{mn}e^{-ik_{szmn}(h-z)}\right)J_1(k_m r), \tag{27}$$

where $h$ is the thickness of the element and $k_{pzmn}$ and $k_{szmn}$ are as defined in Eqs. (19) and (22), respectively. The first term inside the brackets, in both equations, represents the incident wave from $z=0$ and the second represents the reflected wave from the boundary at $z=h$. Upon substituting Eqs. (26) and (27) into Eqs. (6), the following expressions for the radial and vertical displacements are obtained:

$$\hat{u}_{mn}(r,z,k_m,\omega_n) = \begin{pmatrix} -A_{mn}k_m e^{-ik_{pzmn}z} - C_{mn}k_m e^{-ik_{pzmn}(h-z)} \\ +iB_{mn}k_{szmn}e^{-ik_{szmn}z} - iD_{mn}k_{szmn}e^{-ik_{szmn}(h-z)} \end{pmatrix} J_1(k_m r), \tag{28}$$

$$\hat{w}_{mn}(r,z,k_m,\omega_n) = \begin{pmatrix} -iA_{mn}k_{pzmn}e^{-ik_{pzmn}z} + iC_{mn}k_{pzmn}e^{-ik_{pzmn}(h-z)} \\ +B_{mn}k_m e^{-ik_{szmn}z} + D_{mn}k_m e^{-ik_{szmn}(h-z)} \end{pmatrix} J_0(k_m r). \tag{29}$$

Let the radial and vertical displacements for the node at $z=0$ equal $u_1$ and $w_1$ and for the node at $z=h$ equal $u_2$ and $w_2$, respectively, Fig. 3. By applying these boundary conditions on Eqs. (28) and (29), for the

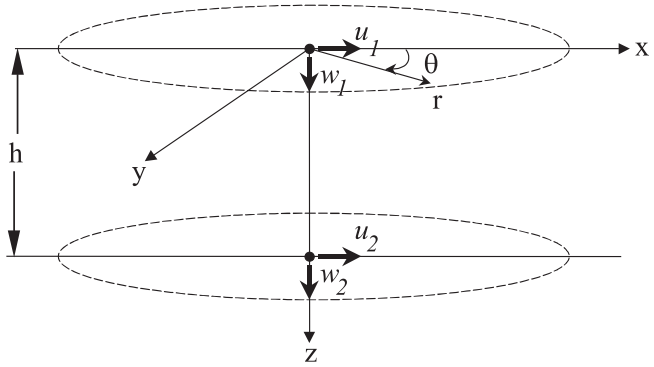


Fig. 3. 2-noded axi-symmetric layer element.

waves travelling in the $z$ direction, a relationship between the coefficients $A_{mn}$, $B_{mn}$, $C_{mn}$ and $D_{mn}$ and the nodal displacements can be obtained as

$$\begin{Bmatrix} \hat{u}_{1mn} \\ \hat{w}_{1mn} \\ \hat{u}_{2mn} \\ \hat{w}_{2mn} \end{Bmatrix} = \begin{bmatrix} -k_m & \mathrm{i}k_{szmn} & -k_m \mathrm{e}^{-\mathrm{i}k_{pzmn}h} & -\mathrm{i}k_{szmn}\mathrm{e}^{-\mathrm{i}k_{szmn}h} \\ -\mathrm{i}k_{pzmn} & k_m & \mathrm{i}k_{pzmn}\mathrm{e}^{-\mathrm{i}k_{pzmn}h} & k_m \mathrm{e}^{-\mathrm{i}k_{szmn}h} \\ -k_m \mathrm{e}^{-\mathrm{i}k_{pzmn}h} & \mathrm{i}k_{szmn}\mathrm{e}^{-\mathrm{i}k_{szmn}h} & -k_m & -\mathrm{i}k_{szmn} \\ -\mathrm{i}k_{pzmn}\mathrm{e}^{-\mathrm{i}k_{pzmn}h} & k_m \mathrm{e}^{-\mathrm{i}k_{szmn}h} & \mathrm{i}k_{pzmn} & k_m \end{bmatrix} \begin{Bmatrix} A_{mn} \\ B_{mn} \\ C_{mn} \\ D_{mn} \end{Bmatrix}. \tag{30}$$

The coefficients $A_{mn}$, $B_{mn}$, $C_{mn}$ and $D_{mn}$ can be determined in terms of the four nodal displacements $\{\hat{u}_{1nm}, \hat{w}_{1nm}, \hat{u}_{2nm}, \hat{w}_{2nm}\}^{\mathrm{T}}$ by inverting Eq. (30). The resulting system of equations can be written symbolically as

$$\{SF_{mn}\} = [\hat{I}_{mn}]\{\hat{\mathrm{D}}\mathrm{ISP}_{mn}\}, \tag{31}$$

where $\{SF_{mn}\}$ represents the coefficients vector, $\left[\hat{I}_{mn}\right]$ represents the inverse of the square matrix of Eq. (30) and $\{\hat{\mathrm{D}}\mathrm{ISP}_{mn}\}$ represents the nodal displacements vector. The explicit form of matrix $\left[\hat{I}_{mn}\right]$ is not included here because its determination requires a simple $4 \times 4$ matrix inverse procedure. $\{SF_{mn}\}$ of Eq. (31), corresponds to the shape functions in the conventional finite element method. However, the shape functions expressed by $\{SF_{mn}\}$ have been determined on the basis of the explicit solution of wave motion equations. Because the mass distribution is expressed exactly, one element only is adequate for the simulation of a whole layer. This feature constitute an essential advantage of the spectral element method over those, which lump the mass at the layer interfaces (or nodes).

Following the Cauchy stress principle, the applied boundary tractions are related to the normal and shear stresses at the boundaries by

$$T_k = \tau_{km}\mathbf{n}_m, \tag{32}$$

where the unit vector $\mathbf{n}$ is perpendicular to the surface and points outwards.

On substituting Eqs. (28) and (29) into Eqs. (7), and by use of Eq. (32), a relationship between the traction and shape functions $\{SF_{mn}\}$ can be obtained as

$$\begin{Bmatrix} \hat{T}_{r1mn} \\ \hat{T}_{z1mn} \\ \hat{T}_{r2mn} \\ \hat{T}_{z2mn} \end{Bmatrix} = \mu \begin{bmatrix} -2\mathrm{i}k_m k_{pzmn} & -\left(k_{szmn}^2 - k_m^2\right) & 2\mathrm{i}k_m k_{pzmn}\mathrm{e}^{-\mathrm{i}k_{pzmn}h} & -\left(k_{szmn}^2 - k_m^2\right)\mathrm{e}^{-\mathrm{i}k_{szmn}h} \\ \left(k_{szmn}^2 - k_m^2\right) & 2\mathrm{i}k_m k_{szmn} & \left(k_{szmn}^2 - k_m^2\right)\mathrm{e}^{-\mathrm{i}k_{pzmn}h} & -2\mathrm{i}k_m k_{szmn}\mathrm{e}^{-\mathrm{i}k_{szmn}h} \\ 2\mathrm{i}k_m k_{pzmn}\mathrm{e}^{-\mathrm{i}k_{pzmn}h} & \left(k_{szmn}^2 - k_m^2\right)\mathrm{e}^{-\mathrm{i}k_{szmn}h} & -2\mathrm{i}k_m k_{pzmn} & \left(k_{szmn}^2 - k_m^2\right) \\ -\left(k_{szmn}^2 - k_m^2\right)\mathrm{e}^{-\mathrm{i}k_{pzmn}h} & -2\mathrm{i}k_m k_{szmn}\mathrm{e}^{-\mathrm{i}k_{szmn}h} & -\left(k_{szmn}^2 - k_m^2\right) & 2\mathrm{i}k_m k_{szmn} \end{bmatrix} \times \begin{Bmatrix} A_{mn} \\ B_{mn} \\ C_{mn} \\ D_{mn} \end{Bmatrix}, \tag{33}$$

where $\mu$ is the Lame constant. If the above $4 \times 4$ matrix is denoted as $\left[\hat{H}_{mn}\right]$, then upon substituting Eq. (31) into Eq. (33), the following relationship between the traction and nodal displacements is obtained:

$$\{\hat{T}_{mn}\} = (\mu[\hat{H}_{mn}][\hat{I}_{mn}])\{\hat{\mathrm{D}}\mathrm{ISP}_{mn}\}. \tag{34}$$

The expression between the parentheses in Eq. (34) relates the nodal displacements with the applied tractions. As in the case of the finite element method, it represents the stiffness matrix of the layer element. The difference between a spectral element stiffness matrix and a conventional finite element stiffness matrix is that the former is frequency and wavenumber dependent.

Upon matrix multiplication of $[\hat{H}_{mn}]$ and $[\hat{I}_{mn}]$, a complex and symmetric $4 \times 4$ dynamic stiffness matrix is obtained as

$$[\hat{k}_{mn}] = \begin{bmatrix} k_{11mn} & k_{12mn} & k_{13mn} & k_{14mn} \\ & k_{22mn} & -k_{14mn} & k_{24mn} \\ & & k_{11mn} & -k_{12mn} \\ sym & & & k_{22mn} \end{bmatrix}, \tag{35}$$

where

$$\begin{aligned}
k_{11mn} &= \frac{\mu}{\Delta_{mn}} \left\{ \mathrm{i}k_{pzmn} \left(k_{szmn}^2 + k_m^2\right) \left(k_m^2 Q_{12} Q_{21} + k_{szmn} k_{pzmn} Q_{11} Q_{22}\right) \right\}, \\
k_{12mn} &= \frac{\mu}{\Delta_{mn}} \left\{ \begin{array}{c} k_m k_{szmn} k_{pzmn} \left( -k_{szmn}^2 + 3k_m^2 \right) \left(Q_{12} Q_{22} - 4\mathrm{e}^{-\mathrm{i}k_{pzmn}h} \mathrm{e}^{-\mathrm{i}k_{szmn}h}\right) \\ -k_m Q_{11} Q_{21} \left(k_m^2 k_{szmn}^2 - k_m^4 - 2k_{pzmn}^2 k_{szmn}^2\right) \end{array} \right\}, \\
k_{13mn} &= \frac{\mu}{\Delta_{mn}} \left\{ -2\mathrm{i}k_{pzmn} \left(k_{szmn}^2 + k_m^2\right) \left(k_m^2 \mathrm{e}^{-\mathrm{i}k_{pzmn}h} Q_{21} + k_{szmn} k_{pzmn} \mathrm{e}^{-\mathrm{i}k_{szmn}h} Q_{11}\right) \right\}, \\
k_{14mn} &= \frac{\mu}{\Delta_{mn}} \left\{ 2k_{szmn} k_{pzmn} \left(k_{szmn}^2 + k_m^2\right) \left(\mathrm{e}^{-\mathrm{i}k_{pzmn}h} Q_{22} - \mathrm{e}^{-\mathrm{i}k_{szmn}h} Q_{12}\right) \right\}, \\
k_{22mn} &= \frac{\mu}{\Delta_{mn}} \left\{ \mathrm{i}k_{szmn} \left(k_{szmn}^2 + k_m^2\right) \left(k_m^2 Q_{11} Q_{22} + k_{szmn} k_{pzmn} Q_{12} Q_{21}\right) \right\}, \\
k_{24mn} &= \frac{\mu}{\Delta_{mn}} \left\{ -2\mathrm{i}k_{szmn} \left(k_{szmn}^2 + k_m^2\right) \left(k_m^2 \mathrm{e}^{-\mathrm{i}k_{szmn}h} Q_{11} + k_{szmn} k_{pzmn} \mathrm{e}^{-\mathrm{i}k_{pzmn}h} Q_{21}\right) \right\}
\end{aligned}$$

in which $\Delta_{mn}$ is the characteristic equation of the layer element defined as

$$\begin{aligned}
\Delta_{mn} &= 2k_m^2 k_{pzmn} k_{szmn} \left(4\mathrm{e}^{-\mathrm{i}k_{pzmn}h} \mathrm{e}^{-\mathrm{i}k_{szmn}h} - Q_{12} Q_{22}\right) - \left(k_{pzmn}^2 k_{szmn}^2 + k_m^4\right) Q_{11} Q_{21}, \\
Q_{11} &= 1 - \mathrm{e}^{-2\mathrm{i}k_{pzmn}h}, \quad Q_{21} = 1 - \mathrm{e}^{-2\mathrm{i}k_{szmn}h}, \quad Q_{12} = 1 + \mathrm{e}^{-2\mathrm{i}k_{pzmn}h}, \quad Q_{22} = 1 + \mathrm{e}^{-2\mathrm{i}k_{szmn}h}.
\end{aligned}$$

### 4.2. 1-Noded half-space element

The 1-noded element is a special case of the 2-noded element. The 1-noded element behaves as a carrier of energy out of the system, in which the waves travel in one direction and no reflection occurs, Fig. 4. In this case, the wave Eqs. (26) and (27) reduce to Eqs. (20) and (21), and the coefficients $C_{mn}$ and $D_{mn}$ in Eqs. (28) and (29) are equal to zero. The kernels of the displacements $\hat{u}$ and $\hat{w}$ are therefore

$$\hat{u}_{mn}(z, k_m, \omega_n) = -A_{mn} k_m \mathrm{e}^{-\mathrm{i}k_{pzmn}z} + \mathrm{i}B_{mn} k_{szmn} \mathrm{e}^{-\mathrm{i}k_{szmn}z}, \tag{36}$$

$$\hat{w}_{mn}(z, k_m, \omega_n) = -\mathrm{i}A_{mn} k_{pzmn} \mathrm{e}^{-\mathrm{i}k_{pzmn}z} + B_{mn} k_m \mathrm{e}^{-\mathrm{i}k_{szmn}z}. \tag{37}$$

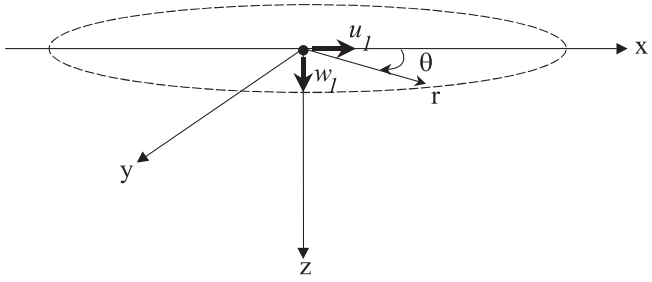


Fig. 4. 1-noded half-space element.

By solving Eqs. (36) and (37) for the coefficients $A_{mn}$ and $B_{mn}$, the shape functions of the 1-noded element can be obtained as

$$\begin{Bmatrix} A_{mn} \\ B_{mn} \end{Bmatrix} = \frac{1}{k_m^2 + k_{pzmn}k_{szmn}} \begin{bmatrix} -k_m & \mathrm{i}k_{szmn} \\ -\mathrm{i}k_{szmn} & k_m \end{bmatrix} \begin{Bmatrix} \hat{u}_{1mn} \\ \hat{w}_{1mn} \end{Bmatrix}. \tag{38}$$

Following the Cauchy stress principle, the tractions at node 1 are related to the stresses by

$$\hat{T}_{z1mn} = -\hat{\sigma}_{z1nm} \quad \text{and} \quad \hat{T}_{r1mn} = -\hat{\tau}_{r1mn}. \tag{39}$$

On substituting Eqs. (36) and (37) into Eqs. (7), and substituting the results into Eq. (39), the following relationships are obtained between the applied traction $\hat{T}_{z1mn}$ and $\hat{T}_{r1mn}$ and the coefficients $A_{mn}$ and $B_{mn}$:

$$\begin{Bmatrix} \hat{T}_{r1mn} \\ \hat{T}_{z1mn} \end{Bmatrix} = \mu \begin{bmatrix} -2\mathrm{i}k_m k_{pzmn} & -\left(k_{szmn}^2 - k_m^2\right) \\ k_{szmn}^2 - k_m^2 & 2\mathrm{i}k_m k_{szmn} \end{bmatrix} \begin{Bmatrix} A_{mn} \\ B_{mn} \end{Bmatrix}. \tag{40}$$

Upon substituting $A_{mn}$ and $B_{mn}$ from Eq. (38) into Eq. (40), the 1-noded half-space element stiffness matrix can be derived as

$$\begin{Bmatrix} \hat{T}_{r1mn} \\ \hat{T}_{z1mn} \end{Bmatrix} = \frac{\mu}{\Delta_{mn}} \begin{bmatrix} \mathrm{i}k_{pzmn}\left(k_{sz}^2 + k_m^2\right) & \left(2k_{pzmn}k_{szmn} - k_{szmn}^2 + k_m^2\right)k_m \\ sym & \mathrm{i}k_{szmn}\left(k_{sz}^2 + k_m^2\right) \end{bmatrix} \begin{Bmatrix} \hat{u}_{1mn} \\ \hat{w}_{1mn} \end{Bmatrix}, \tag{41}$$

where $\Delta_{mn} = k_m^2 + k_{pzmn}k_{szmn}$.

### 4.3. Spectral structural stiffness matrix assemblage and system solution

The spectral structural stiffness matrix $\left[\hat{K}(k_m, \omega_n)\right]$ must be assembled at each frequency and wavenumber. Assemblage of $\left[\hat{K}(k_m, \omega_n)\right]$ follows the same procedures as that of the conventional finite element method (Cook, 1974). Same is valid for the assemblage of the global force vector. The global system of equations to be solved is therefore

$$\begin{Bmatrix} \hat{u}_{1mn} \\ \hat{w}_{1mn} \\ \vdots \\ \hat{u}_{lmn} \\ \hat{w}_{lmn} \end{Bmatrix} \begin{bmatrix} \\ \hat{K}(k_m, \omega_n) \\ \\ \end{bmatrix} = \begin{Bmatrix} \hat{P}_{r1mn} \\ \hat{P}_{z1mn} \\ \vdots \\ \hat{P}_{rlmn} \\ \hat{P}_{zlmn} \end{Bmatrix}, \tag{42}$$

in which $l$ represents an element number. The vector in the left hand side is the displacement vector and the one in the right hand side is the force vector. The relationship between the force $\hat{P}_{zlmn}$ and the tractions at the node located, say for example, between element $l$ and $l-1$ is

$$\hat{P}_{zlmn} = A \times \left(\hat{T}_{z2mn}^{(l-1)} + \hat{T}_{z1mn}^{(l)}\right)$$

in which $A$ is the area of the applied load. If a normal load is applied at node 1 of element 1 (at the surface), which is usually the case, then $\hat{P}_{z1mn} = A \times \hat{T}_{z1mn}^{(1)}$.

Similar to the conventional finite element stiffness matrix, $\left[\hat{K}(k_m, \omega_n)\right]$ is symmetric and banded. However, the spectral stiffness matrix is complex and hence exhibits a damped behaviour in the time domain. Its inverse denotes $\hat{G}(k_m, z)$ of Eq. (25).

By considering the solution of harmonic loading, the solution to the case of arbitrary time variation can be obtained by means of the FFT. The solution to the spatial variation of the load can be introduced by means of the Fourier–Bessel superposition. Solution of Eq. (42) for a load varying in space and time can be obtained by the following procedure:

- Upon assemblage of $\left[\hat{K}(k_m,\omega_n)\right]$, for a given frequency, the nodal displacement vector of Eq. (42) is computed for a unit load applied at the node of interest. The process is repeated $M$ times for each frequency.
- For the actually applied load $P(r,t)$, with spatial distribution $S(r)$ and time variation $F(t)$, the actual displacements are obtained by scaling the above computed displacements with Fourier coefficient amplitudes of the spatial and time distributions of the load. Summation over all $M$ and $N$ is necessary

$$u(r,z,t)=\sum_n\sum_m \hat{u}_{mn}(z,k_m,\omega_n)\hat{F}_m J_1(k_m r)\hat{F}_n e^{i\omega_n t}, \tag{43}$$

$$w(r,z,t)=\sum_n\sum_m \hat{w}_{mn}(z,k_m,\omega_n)\hat{F}_m J_0(k_m r)\hat{F}_n e^{i\omega_n t}, \tag{44}$$

where $\hat{F}_m$ represents the Fourier–Bessel coefficients of $S(r)$ and $\hat{F}_n$ denotes the fast Fourier coefficients of $F(t)$. Their combination denotes $\hat{P}_{mn}$ of Eq. (25).

### 4.4. Determination of $\hat{F}_n$ and $\hat{F}_m$

The Fourier coefficients $\hat{F}_n$ can be obtained by means of FFT. The numerical scheme presented by Brigham (1988), which is based on the Cooley–Tukey of the Base-2 FFT algorithm, is utilized. Here, the discrete Fourier transform pair for $F(t)$ and $\hat{F}_n$ is given by

$$F(t_k)=\frac{1}{N}\sum_n \hat{F}_n\left(\frac{n}{N\cdot\Delta t}\right)e^{i\omega_n t_k}=\frac{1}{N}\sum_n \hat{F}_n\left(\frac{n}{N\cdot\Delta t}\right)e^{i2\pi nk/N}, \tag{45a}$$

$$\hat{F}_n\left(\frac{n}{N\cdot\Delta t}\right)=\sum_k F(t_k)e^{-i\omega_n t_k}=\sum_k F(t_k)e^{-i2\pi nk/N}, \tag{45b}$$

where both $k$ and $n$ range from 0 to $N-1$, $N$ is the number of samples to the Nyquist frequency, $\Delta t$ is the sampling interval and $t_k=k\cdot\Delta t$.

The $\hat{F}_m$ components, on the other hand, can be obtained by use of the Fourier–Bessel theory. For a cylindrical shape load (Fig. 5 (a)), with radius $a$ and amplitude $q$, $S(r)$ may be expressed as

$$S(r)=\begin{cases} q & \text{for } 0\leqslant r\leqslant a,\\ 0 & \text{for } a<r\leqslant R,\end{cases} \tag{46}$$

where $R$ is the radial dimension of the structure ($R$ is taken relatively large to insure that $u$ and $w$ in Eqs. (43) and (44) are equal to zero). Expressing $S(r)$ by means of Fourier–Bessel series

$$S(r)=\sum_m \hat{F}_m J_0(k_m r), \tag{47}$$

the coefficient $\hat{F}_m$ for a cylindrical shape with height $q=1$ and radius $a$ can be determined analytically (Kreyszig, 1999) as

$$\hat{F}_m=\frac{2}{R^2 J_1^2(\alpha_m)}\int_0^a r J_0\left(\frac{\alpha_m}{R}r\right)dr. \tag{48}$$

where, $\alpha_m$ denotes the roots of the Bessel function $J_0$. After evaluation of the integral, Eq. (48) reduces to

$$\hat{F}_m=\frac{2a}{\alpha_m R J_1^2(\alpha_m)}J_1\left(\frac{\alpha_m}{R}a\right). \tag{49}$$

The Fourier–Bessel series of the circular load of Fig. 5(a) for $a=0.15$ m and $R=25$ m is presented in Fig. 5(b) for $M=1700$.

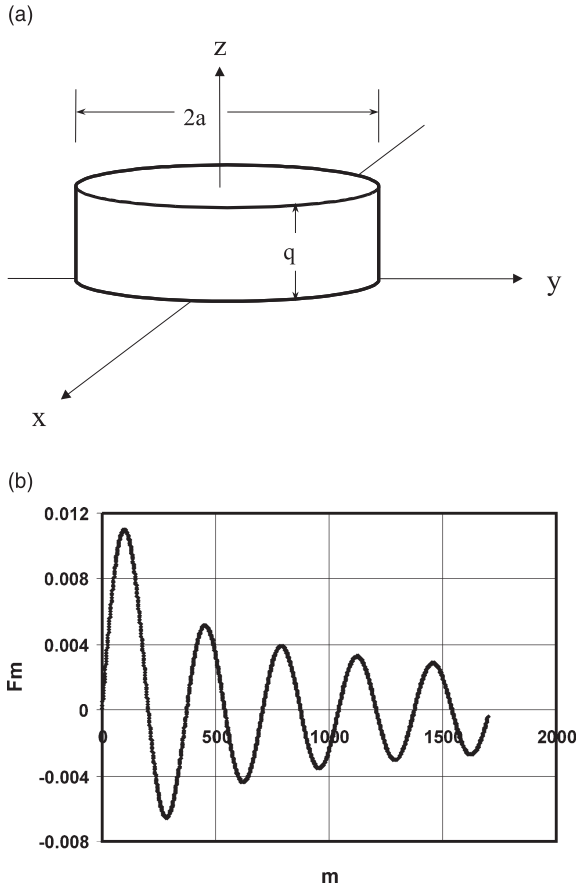


Fig. 5. (a) Load shape and (b) Fourier–Bessel distribution.

## 5. Numerical implementation

The above-formulated axi-symmetric spectral elements for a layer and a half-space have been implemented in the computer program layered media dynamics analysis (LAMDA) developed at TU-Delft. The algorithm of the program is presented in Fig. 6.

The algorithm consists of three main steps: pre-processing (box 1), main program (boxes 2–9) and post-processing (box 10). In the pre-processing step, the input force is transformed from the time domain to the frequency domain. Here, $\hat{F}_n$ is calculated based on Eq. (45b), by use of the FFT algorithm. The main program involves two loops over $N$ frequencies and $M$ wavenumbers. For any given combination of frequency and wavenumber the structural stiffness matrix is formed and inverted (box 4). Displacements under a unit load (on node 1 in the FWD case) are computed at each node, box 5. (The $j$ between brackets in box 5 denotes the node number.) In box 7, summation over the wavenumbers is done to compute $M$ modal responses at a specific frequency $\omega_n$. Here, $\hat{F}_m$ is computed by means of Eq. (49). Summation over $N$ frequencies is done in box 9. In the post-processing step (box 10), inversion back to the time domain is done by means of FFT (Eq. (45a)).

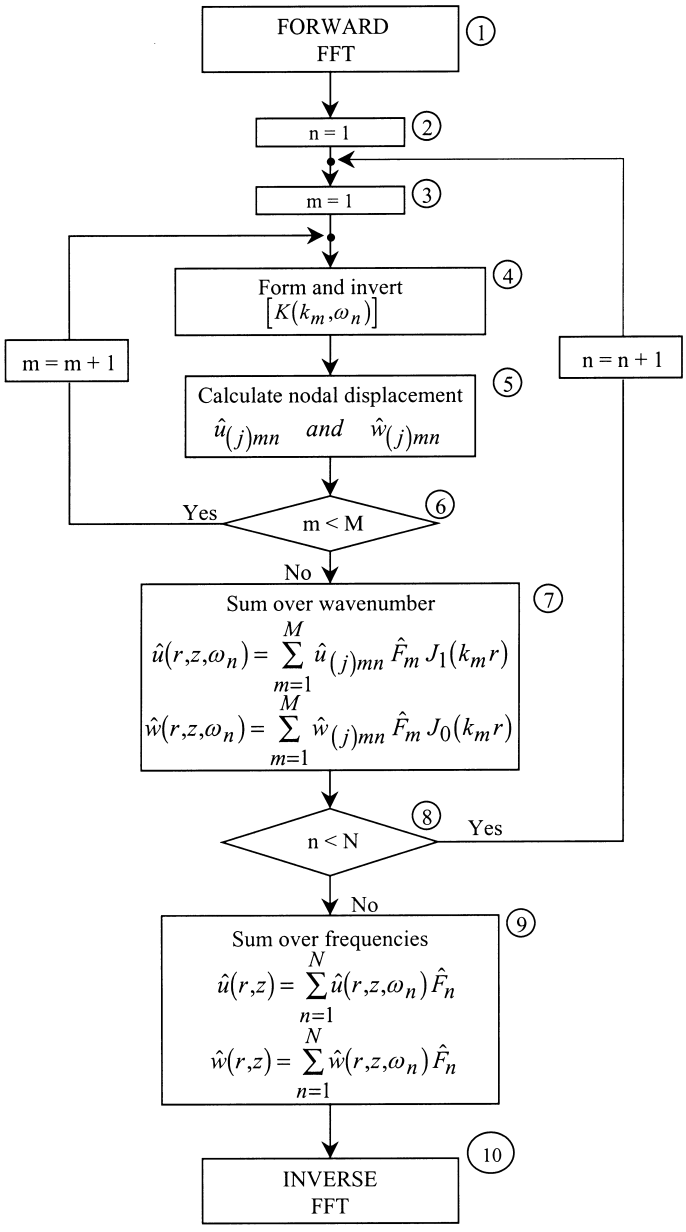


Fig. 6. LAMDA computer program flow chart.

## 6. Element verification

Verification of the axi-symmetric spectral element formulations and their numerical implementation has been done by comparing the results with that of the finite element method and the multi-layered stiffness matrix method of Kausel and Roesset.

The finite element system CAPA-3D (Scarpas, 1993) was utilized for this purpose. It can perform static/dynamic linear/non-linear analysis. A typical pavement structure consisting of three layers; asphalt, subbase

and subgrade was chosen for this purpose. The geometrical and material properties are presented in Table 1. The pavement is subjected to a 50 kN FWD load pulse with 25 ms duration and 150 mm radius.

Table 1
Geometrical and material properties

| | Thickness (mm) | $E$ modulus (MPa) | Poisson's ratio | Mass density (kg/m$^3$) |
|---|---|---|---|---|
| Asphalt | 150 | 1000 | 0.35 | 2300 |
| Subbase | 250 | 200 | 0.35 | 2000 |
| Subgrade | $\infty$ | 100 | 0.35 | 1500 |

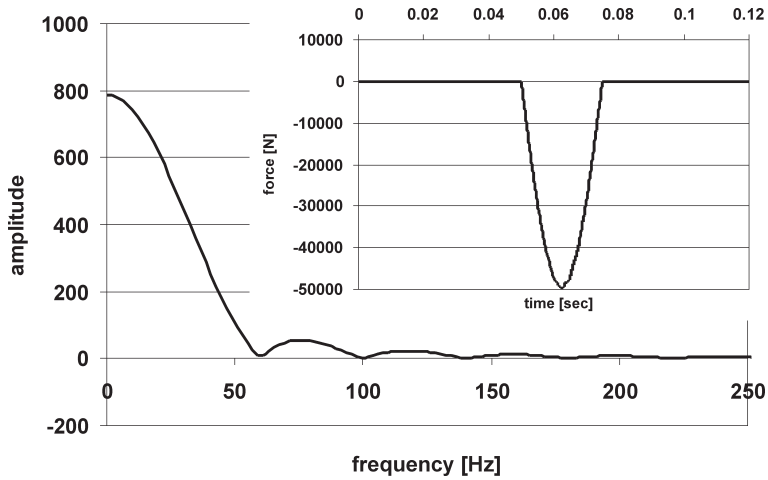


Fig. 7. FWD load pulse and its spectrum.

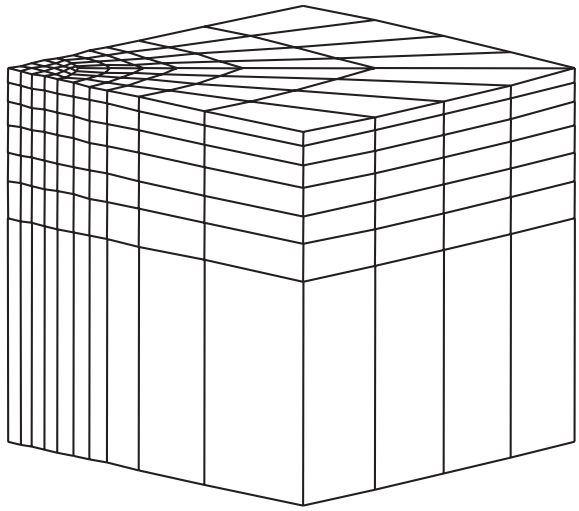

Fig. 8. Finite element mesh.

In LAMDA, the geometry was simulated by the use of two layer elements and one half-space element. The time history of the load pulse $F(t)$ and its frequency spectrum are shown in Fig. 7. The spatial distribution $S(r)$ is given by the cylindrical shape shown in Fig. 5(a) with radius $a = 150$ mm.

In the finite element system CAPA-3D, the geometry was simulated by use of 1040, 20 noded brick elements. Because of the required finite geometry, the structure was assumed to extend 6 m in the horizontal direction and 15.4 m in the vertical direction. Also, because of axi-symmetry, only a quadrant of the pavement was simulated. The radius of the loaded area was 150 mm. The detailed mesh surrounding the loaded area is shown in Fig. 8.

The oscillation of the pavement surface, at several geophone locations, as computed by CAPA-3D is presented in Fig. 9(a) and by LAMDA in Fig. 9(b). It can be seen that the results are similar except that in the finite element analysis some disturbances appear at the end of the response, which can be attributed to the reflections at the boundaries of the mesh.

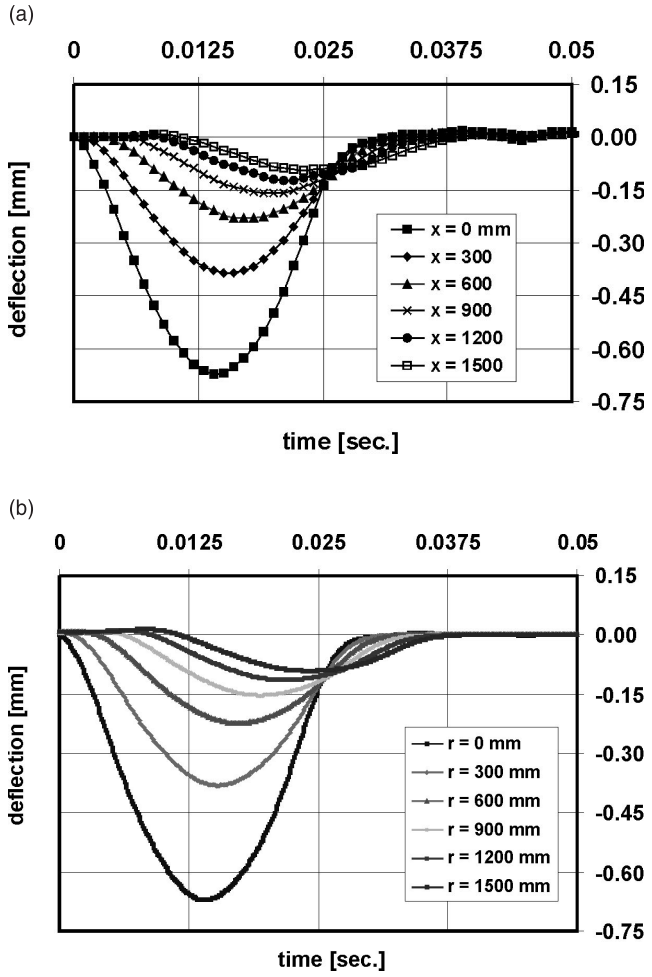


Fig. 9. Pavement surface oscillations: (a) CAPA-3d and (b) LAMDA.

The advantage of the spectral elements method lies in its moderate input and computational requirements compared with the finite element method. For the above analyses, the computational requirements for both methods are summarized in Table 2.

Table 2
Computational requirements

| Method | Mesh size | Computational time | Computer type |
|---|---|---|---|
| Finite elements | 1040 | 3 h | Alpha station 200 |
| Spectral elements | 3 | 50 s | Intel 300 MHz |

Table 3
Geometrical and material properties of Foinquinos et al. (1995)

| Layer | Thickness (cm) | Young's Modulus (MPa) | Shear-wave velocity (m/s) |
|---|---|---|---|
| Asphalt | 15 | 3013 | 762 |
| Base | 30 | 483 | 305 |
| Subgrade | Variable | 124 | 152 |

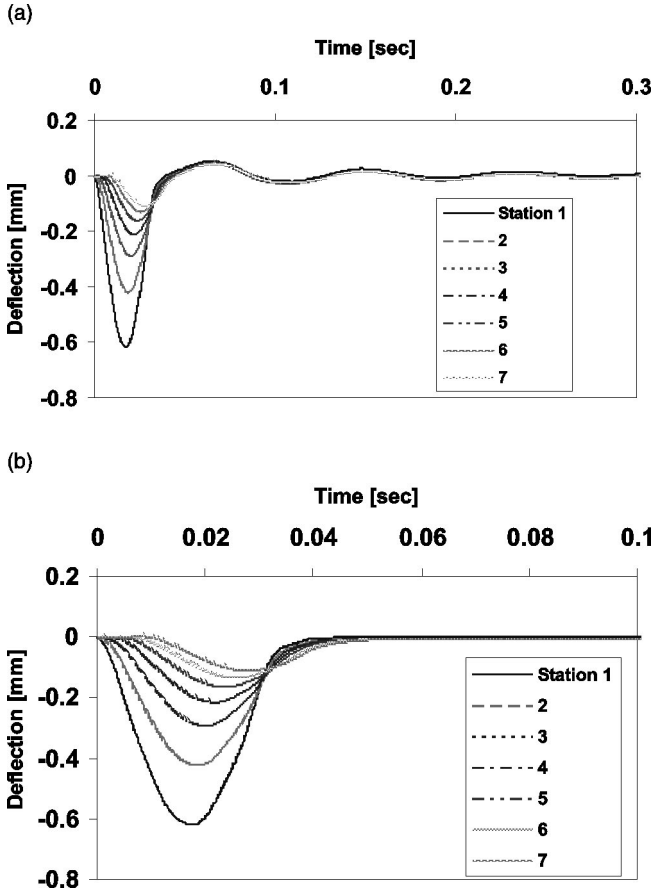


Fig. 10. LAMDA results: (a) Bed rock at 6.1 m and (b) no bed rock.

The results obtained from the spectral element method had also been compared with the multi-layered stiffness matrix method developed by Kausel and Roesset (1981). For this purpose, the work presented by Foinquinos et al. (1995), which involves comprehensive use of the method to FWD test simulation, is utilized. A flexible pavement structure consisting of three layers; asphalt, base and subgrade was simulated. The material elastic properties and layer thickness are presented in Table 3. An FWD load pulse of 90 kN and 30 ms was used as input. Two different subgrade conditions were analysed; rockbed at 6 m depth and infinite soft soil. LAMDA results for both cases are presented in Fig. 10. A comparison with those of Fig. 3 of Foinquinos, shows that they are identical (same format as that in Foinquinos et al. (1995) was used for closer comparison).

## 7. Conclusions

The spectral element method has been shown to be an efficient computational tool for analyzing the dynamic response of multi-layered systems when subjected to a transient load pulse. Comparison with finite element analysis of some typical pavements under FWD load action and with computational results obtained by use of the layer stiffness matrix method of Kausel and Roesset, the axi-symmetric spectral elements, developed and implemented in this research work, have shown to be accurate.

The main advantage of the spectral element method over other layered media formulations lies on its computational efficiency and robustness. The double summation approach of the spectral element evades the inconvenience of the numerical evaluation of contour integration between zero and infinity, which results, in many practical applications, to numerical oscillations.

Because waves are described exactly in the spectral element method, one element is adequate to describe a whole layer. Consequently, the size of the mesh of a layered structure is only as large as the number of the layers involved. This reduces the computational requirements dramatically and encourages utilization of this method for parameter identification purposes, which will be addressed in a subsequent contribution.

## Acknowledgements

This work is funded by the European Commission under the Transport TRD Program of the fourth Framework Program under a project name "SpecifiQ". The authors are grateful to the SpecifiQ project leader Dr. C. van Gurp for the many discussions and insight he has provided in the course of the project.

## References

Abramowitz, M., Stegun, I.A., 1972. Handbook of Mathematical Functions. Dover Publication, New York.
Achenbach, J.D., 1973. Wave Propagation in Elastic Solids. North-Holland, The Netherlands.
Brigham, E.O., 1988. The Fast Fourier Transform and Its Applications. Prentice-Hall, Englewood Cliffs, NJ.
Cook, R.D., 1974. Concepts and Applications of Finite Element Analysis. Wiley, New York.
Doyle, J.F., 1997. Wave Propagation in Structures: Spectral Analysis Using Fast Discrete Fourier Transforms. Springer, New York.
Foinquinos, R., Roesset, J.M., Stokoe II, K.H., 1995. Response of Pavement Systems to Dynamic Loads Imposed by Nondestructive Tests. In: Transportation Research Record 1504, TRB, National Research Council, Washington, DC, pp. 57–67.
Haskell, N.A., 1953. The dispersion of surface waves on multilayered media. Bull. Seism. Soc. Am. 43, 17–34.
Kausel, E., Roesset, J.M., 1981. Stiffness matrices for layered soils. Bull. Seism. Soc. Am. 71, 1743–1761.
Kreyszig, E., 1999. Advanced Engineering Mathematics. Wiley, New York.
Lysmer, J., 1970. Lumped mass method for Rayleigh waves. Bull. Seism. Soc. Am. 60, 89–104.
Rizzi, S.A., Doyle, J.F., 1992. A spectral element approach to wave motion in layered solids. J. Vibr. Acous. 114, 569–577.

Scarpas, A., 1993. CAPA-3D Finite Elements System-User's Manual Parts I, II and III. Section of Structural Mechanics, Faculty of Civil Engineering and Geosciences, TU-Delft, The Netherlands.

Tassoulas, J.L., Kausel, E., 1983. Elements for the numerical analysis of wave motion in layered strata. Int. J. Numer. Meth. Engng. 19, 1005–1032.

Thomson, W.T., 1950. Transmission of elastic waves through a stratified solid media. J. Applied Phys. 21, 89–93.

Van Gurp, C., 1995. Characterization of Seasonal Influences on Asphalt Pavements with the use of Falling Weight Deflectometers. CIP, Delft, The Netherlands.